A Computational Model of a Centrifugal Compressor Stage for Aircraft Engines

Ing. David Hlaváček

Thesis supervised by: doc. Ing. Daniel Hanus, CSc., EUR ING., AFAIAA

Abstract
This paper presents the ongoing first steps of development of an innovative centrifugal compressor stage designed for use in turboprop aircraft engines. The so-called tandem impeller blading concept shall be compared to the conventional blading design by means of numerical simulation and optimized to achieve the best possible parameters. In this paper, validation of a conventional stage computational model using experimental data is described.

Keywords
centrifugal compressor, turboprop engine. impeller, vaned diffuser, secondary flow, CFD

1 Introduction

Centrifugal compressors are often used in small-sized turboprop, turboshaft and propfan engines as the last compressor stages. Their application in these types of engines brings several advantages. A centrifugal compressor stage usually achieves a substantially higher pressure ratio compared to an axial stage of the same mass flow rate. Therefore, a centrifugal compressor covers much less axial space than four or five axial stages of the same pressure ratio. Moreover, small centrifugal compressor stages often achieve a greater isentropic efficiency than axial stages when used as the last stages. This is caused by lower mass flow rates in smaller engines which, together with decreasing the chord length in the last axial compressor stages, lead to lower values of Reynolds number. This means that viscous forces play a more significant role in the flow field, thus reducing the efficiency of such axial stage.

Fig. 1. *M602 High pressure compressor impeller [7]*

Using a centrifugal stage, on the other hand, does not negatively affect the Reynolds number.

This paper presents a new approach to centrifugal compressor design which will allow certain types of engines to work with an increased efficiency and thus improve their fuel consumption. The tandem-bladed impeller (described below) will be compared to a conventional impeller to prove the advantages of the new concept. In the first stage of development, described in this paper, the computational model of the conventional stage must be compared to the experimental data available. Afterwards, the stage with the tandem-bladed impeller will be modeled.

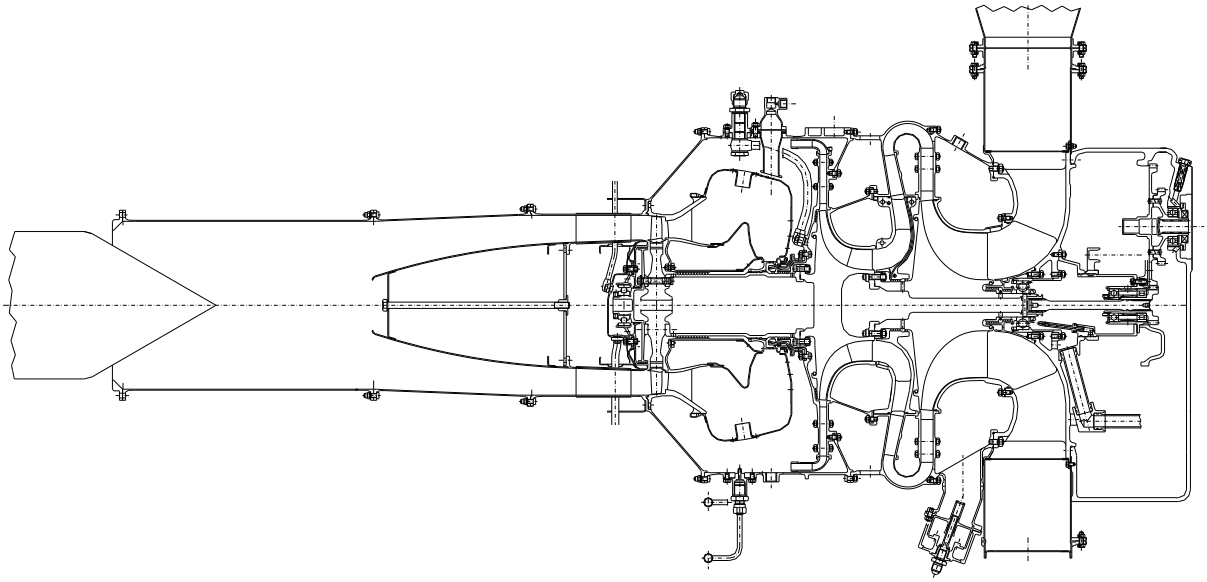

Fig. 2. *M 602 centrifugal compressor test rig. Left, high pressure stage. Right, low pressure stage [7].*

2 Development of the tandem-bladed compressor stage

2.1 Previous development

The conventional compressor stage concerned was developed for the M602 turboprop engine by Walter Engines (now GE Aviation Czech) and VZLÚ (Aerospace Research and Test Establishment). The compressor of this two-shaft engine consisted of two subsequent centrifugal stages (low-pressure and high-pressure compressor).

The novel high-pressure centrifugal compressor stage will use so-called tandem impeller blading. This means that the impeller blades are transversely divided in two parts after the inducer (see Fig. 3 and Fig. 4). The inducer part of the blades is thus made up of an axial blade vane while the exducer part consists of standard radial blading, including splitter blades. The trailing edges of the inducer blades are placed in half the pitch of every second exducer passage. This arrangement positively affects the formation of boundary layers on the impeller blade surfaces. After the inducer parts of the blades, its growth is interrupted and the resulting wake flow is directed into the middle of the downstream exducer channel (**Fig. 4**). This

should result in reducing the size of the wake region at the impeller exit which, in turn, leads to increasing the compressor stage isentropic efficiency. This assumption has already been confirmed by preliminary calculations made in the Institute of Aerospace Engineering, CTU in Prague, which were presented at the ISABE 2005 Conference in München [7].

Fig. 3. *A study of a tandem-bladed impeller [7]*

The previous computations were based on an advanced conventional centrifugal compressor stage designed by Walter Engines. This stage was first examined experimentally and its performance curve was measured. Then a CFD calculation of this conventional stage was made so as to validate the computational model. Afterwards, the blading of this stage's impeller was changed to the tandem arrangement and calculations were performed using a similar mesh and the same boundary conditions. These calculations showed that a lower total temperature rise was achieved by the tandem-bladed stage, proving that the assumption of increasing the compressor stage efficiency was correct.

The calculations of the relative velocity field have also shown the positive effect of directing the wake behind the inducer part of the blades into the exducer channel (Fig. 4).

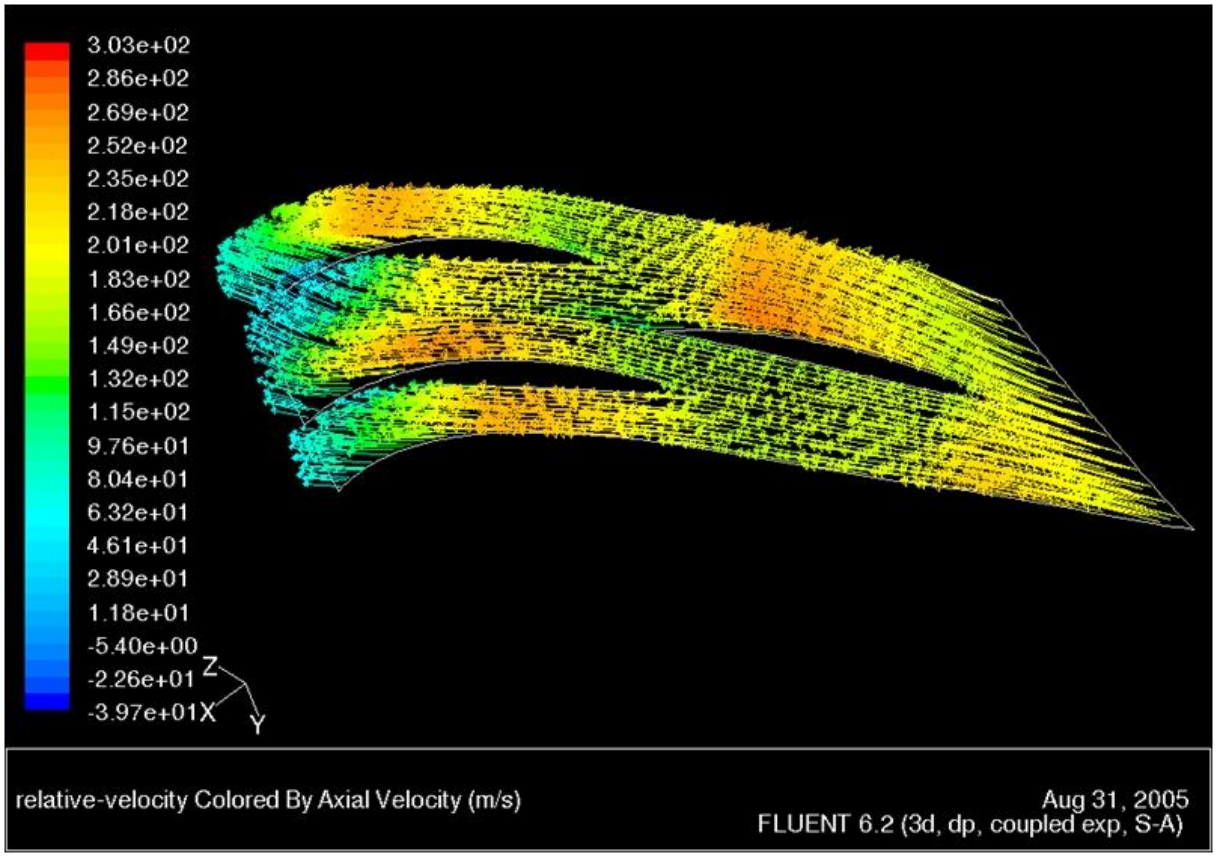

Fig. 4. *Vectors of relative velocity in a cylindrical layer of the tandem-bladed impeller (a previous calculation) [7]*

However, no further steps in improving the tandem-bladed impeller geometry were made. The tandem-bladed impeller was therefore not optimized to achieve the best parameters possible.

The goal of the present research is to find optimal geometries to achieve the highest centrifugal compressor stage isentropic efficiency, highest pressure ratio and the widest mass flow range of stability. A design methodology to achieve such optima should also be developed.

2.2 Recent development

Until now, a CAD model of the whole compressor stage (which includes the impeller, the vaneless and vaned diffusers, and the outlet channel) was converted to geometric models used by the ANSYS computational package and the first calculations aiming at calibrating the computed compressor performance curve with the experimental one were carried out.

The data obtained by these computations should indicate if the computational model describes the existing compressor stage accurately enough. Based on this knowledge, the tandem blades will be modeled optimized computationally.

3 Computational model settings

First of all, the design point of the compressor stage was considered (the design point parameters are given in **Tab. 1**).

Tab. 1. *HP compressor design point parameters*

Total pressure ratio	2.407
Mass flow rate	4.301 $kg.s^{-1}$
Isentropic efficiency	80.5 %
Total temperature rise	162.0 K

The boundary conditions in the compressor design point were set according to the recommendations given in [6]. The authors of this paper claim that different boundary conditions should be chosen in the two respective regions of the performance curve (see Fig. 5). In the left part (near surge condition), the total pressure inlet – mass flow outlet combination should be more accurate since in this nearly horizontal part of the curve, a substantial change of mass flow rate corresponds to a small change of outlet total pressure. On the other hand, in the right part of the performance curve (near choke condition), a combination of boundary conditions prescribing the mass flow at the compressor inlet and the static pressure at the outlet should be used. This is because, in opposition to the left part of the performance curve, large variations of total pressure ratio correspond to small changes of mass flow rate. Therefore, this combination of boundary conditions was used for the compressor design point lying in the right, near-vertical part of the performance curve.

For describing the properties of air, a semi-ideal gas model was used in which the constant pressure specific heat capacity c_p and the dynamic viscosity μ depend on temperature. The functions to determine these dependencies were taken from [4].

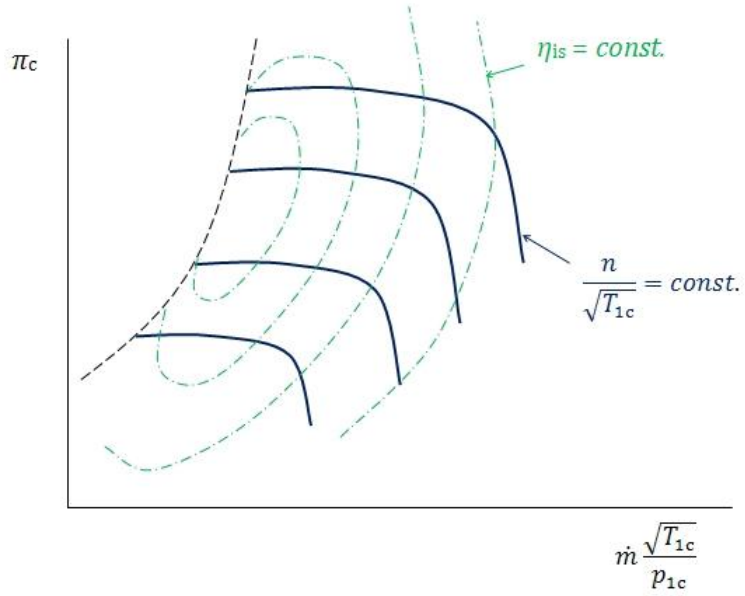

Fig. 5. *A typical compressor map*

The constant pressure specific heat capacity is computed according to a linear formula:

$$\frac{c_p}{R} = a_1 + a_2.T \tag{1}$$

in which R = 8 341 J.kg^{-1}, a_1 = 3.27149, and a_2 = 6.85475444×10^{-4}, while the Sutherland model is used for the dynamic viscosity:

$$\frac{\mu}{\mu_0} = \frac{T_{ref} + S}{T + S}\left(\frac{T}{T_{ref}}\right)^n \tag{2}$$

where μ_0 = 1.712×10^{-5}, T_{ref} = 273 K, S = 111 K, and n = 1.5.

Another important issue to be taken into account, when modeling air flow in a centrifugal compressor stage, is the turbulence model. According to recommendations given by the authors of [1], the RNG k-ε model was chosen which provides a reasonable accuracy without investing an excessive amount of computational time. In [1], the RNG k-ε model was compared to the standard k-ε model and the more sophisticated Reynolds Stress Model (RSM).

The standard k-ε turbulence model is a two-equation model which is based on eddy viscosity concept. In its denomination, k stands for turbulent kinetic energy while ε stands for turbulent eddy dissipation. This model belongs to a group of turbulent viscosity models.

Therefore, the effective viscosity in the momentum equation is a sum of dynamic and turbulent viscosities:

$$\mu_{\text{eff}} = \mu + \mu_{\text{t}} \tag{3}$$

The turbulent viscosity is then computed using the turbulent kinetic energy and turbulent eddy dissipation:

$$\mu_{\text{t}} = C_{\mu} \frac{k^2}{\varepsilon} \tag{4}$$

C_{μ} being a constant (C_{μ} = 0.09 by default).

Since two more unknown quantities are introduced into the system of equations, two additional transport equations need to be solved, one for k, and the other for ε.

The RNG k-ε model uses different values for constants in the transport equation for turbulence eddy dissipation than the standard k-ε model.

As the k-ε turbulence model does not correctly describe the fluid flow in the near-wall region in which viscous forces dominate, a suitable wall function should be chosen to model the near-wall flow field. As a default, a scalable wall function was set.

Based on empirical formulae, wall functions are used for modeling flow field near walls without the need of solving flow in the boundary layer, thus saving computational time. The viscous sublayer which is closest to the wall (see **Fig. 6**) is modeled by the empirical formulae and the nearest computational node is assumed to already lie in the fully-turbulent region of the boundary layer [3].

In addition to the recommendations concerning choice of the most suitable turbulence model, the values of inlet turbulent parameters suitable for modeling flow in small-sized centrifugal compressor stages are provided in [1]. Thus, a turbulence intensity of 5% along with a turbulent length scale of 10 mm was set at the compressor inlet.

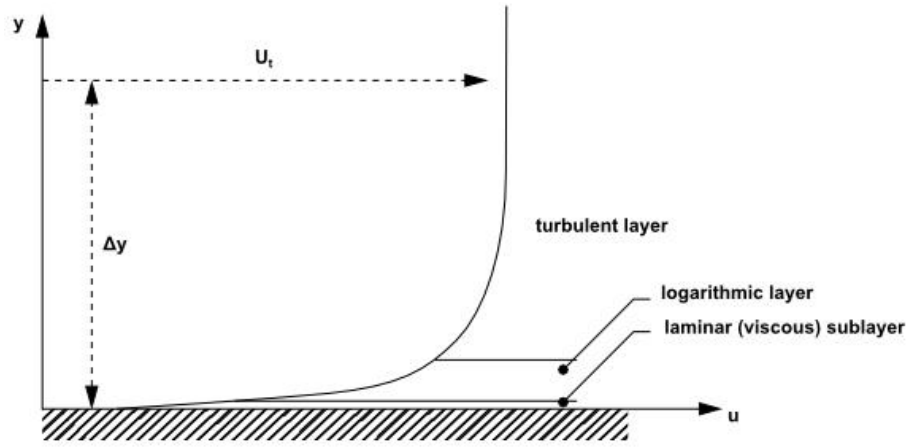

Fig. 6. *A scheme of near-wall flow layers [2]*

Since the flow inside a centrifugal compressor stage is always unsteady and involves both rotating and stationary reference frames, a question of modeling the interface between the impeller and diffuser is of significant importance. A comparison of various approaches to modeling this interface can be found in [8]. In the first computations, the flow was considered to be steady, which, according to [8], can be a reasonable approximation, widely used in practice.

For steady computational models, two types of impeller-diffuser interface models are available in ANSYS CFX: the mixing plane model (named *Stage*) and the *frozen rotor* model. As described in [5], the mixing plane model is based on circumferential averaging of flow quantities at the impeller exit, assuming that the losses caused by circumferential mixing are equal to those which arise during a gradual mixing process inside the diffuser. Thus the flow disturbances which develop inside the impeller vanes do not transfer to the downstream diffuser. Although this assumption is incorrect, the mixing plane model is frequently used in turbomachinery development.

In opposition to the mixing plane model, the frozen rotor model does transfer flow disturbances across the impeller-diffuser interface. The drawback of this approach is that it only does so at one instance in time so the unsteady nature of the flow is not captured correctly. In [8], the two above-mentioned stationary models are compared to the unsteady *transient sliding mesh* model, the mixing plane model being more accurate that the frozen rotor. Therefore, the mixing plane model was used in our case.

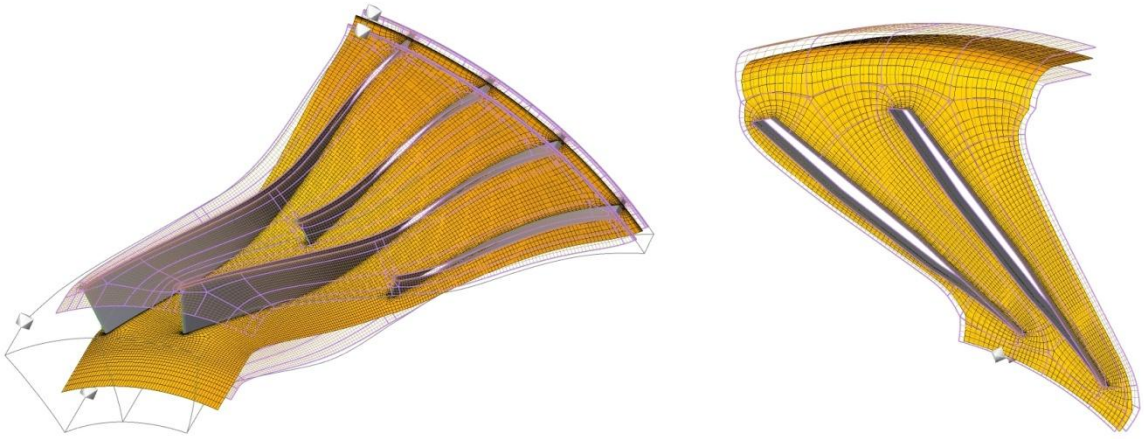

Fig. 7. *Left, the impeller computational mesh. Right, the diffuser mesh*

The 3D mesh (see **Fig. 7**) was generated in ANSYS TurboGrid. For the reason of saving computational time during the calibration process which involves a lot of computational runs, one impeller channel together with one diffuser channel is modeled. Since 16 impeller vanes and 25 diffuser vanes are used in the compressor stage concerned, one impeller pitch is different from one diffuser pitch. In these cases, ANSYS CFX automatically changes the scale of the downstream (diffuser) vane. If two impeller vanes together with three diffuser vanes are used, the pitch ratio nearly equals one and the scale change of the diffuser vanes is considerably smaller. On the other hand, the computational time is correspondingly longer

and it was tested that modeling 2+3 vanes instead of 1+1 vane does not significantly influence the results obtained.

4 Results and discussion

4.1 Stage integral quantities

Three calculations have been made so far: One in the design point and the other two in the left part of the performance curve. For each of these calculations, the same mesh generated by ANSYS TurboGrid was used.

Tab. 2. *Results of computation - integral quantities*

	Design Pt.		Point No. 2		Point No. 3	
	CFX	Measured	CFX	Measured	CFX	Measured
Mass flow rate [kg.s^{-1}]	4.301	4.301	4.000	4.000	3.800	3.800
Total pressure ratio	2.407	2.407	2.645	2.715	2.643	2.750
Isentropic eff. [%]	78.7	80.5	86.6	-	85.8	-
Total temp. rise [K]	171.9	162.0	175.4	-	177.0	-

Due to the fact that the only source of experimental data available at this time from the high-pressure compressor is the measured performance curve, the total temperature rise and isentropic efficiency in points No. 2 and 3 can not be compared to the experimental data.

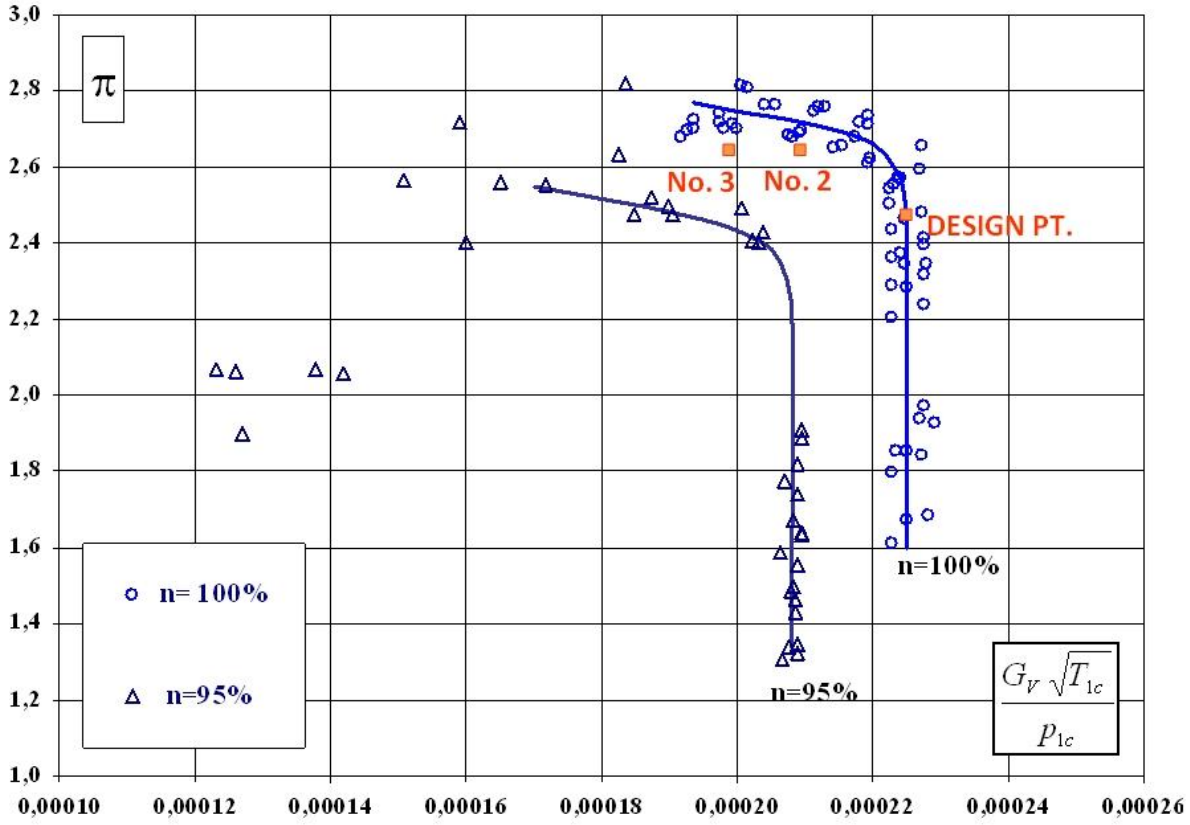

Fig. 8. *A comparison of the computed points to the measured performance curve*

As can be seen from **Tab. 2**and **Fig. 8**, the computation captures the isentropic efficiency and total temperature rise in the design point with an error of 2.23% and 6.1%, respectively. This indicates that the design point isentropic efficiency is underestimated by this model.

In the left part of the performance curve in which the combination of inlet total pressure and outlet mass flow rate was used, the model underestimates the mean value of total pressure ratio by 2.58 % in Point No.2 and by 3.89 % in Point No.3. Even so, the deviation from the lowest measured values is negligible (see **Fig. 8**).

Since the total pressure values computed are lower than those measured, it can be supposed that the computational model overestimates the total pressure losses occurring inside the compressor stage.

A conclusion can be made that the computational model must be refined in order to fit the measured performance curve more closely.

The values of y^+ obtained by the solution (see Tab. 3) show that especially the vaned diffuser mesh should be refined. The dimensionless distance from the wall y^+ used in this evaluation is computed from the following formula:

$$y^+ = y\frac{u^*}{\nu}; \quad \text{in which} \quad u^* = \sqrt{\frac{\tau_w}{\rho}} \qquad \text{(5 a, b)}$$

It is the common formula, not the model-specific one which is also used by CFX.

The authors of [1] claim that, when modelling flow inside turbomachines, the values of y^+ higher than 200 should be avoided and that the law-of-the-wall functions best for y^+ between 30 and 60. According to this statement, the impeller mesh can still be considered sufficient while the diffuser mesh is too coarse.

Tab. 3. *Results of computation - y+ average values*

	Impeller	**Diffuser**
Blade y^+ (area ave.)	176.1	335.9
Domain y^+ (volume ave.)	144.9	786.0

The inaccuracy of the diffuser mesh is also evident from the numbers of cells. As stated above, the mesh was generated in ANSYS TurboGrid using the default settings. One impeller channel was modeled using 250,212 cells, one diffuser channel being made up of just 30,000 cells.

Therefore, the diffuser mesh should be refined in the first step. Afterwards, in order to further refine the computations, a more accurate boundary layer model should be used considering the fact that the flow inside centrifugal compressor stages is dominated by viscous effects and flow separations are to be expected even in the design point. The locations of flow separation should then be predicted more precisely than with the use of the wall function.

4.2 Flow field inside the impeller

The static and total pressure distribution at the impeller outlet (**Fig. 10**) shows typical jet-wake velocity patterns developing in both sets of channels (Main P.S. – Splitter S.S. and Main S.S. – Splitter P.S.) with wake zones close to the shroud and suction sides of both sets of blades. It can be seen that the pressure patterns are different in each set of channels. During further development of this compressor stage, achieving a uniform appearance of pressure patterns in both sets of channels is advisable. This would lead to reducing the mixing losses inside the diffuser.

The same phenomena are visible in **Fig. 9** which shows the relative velocity vectors at the impeller outlet.

The sharper difference between the minimum and maximum pressure in the Main Blade P.S. – Splitter S.S. channel is caused by the fact that the tip leakage mass flow is greater on the main blade tip than on the splitter blade tip. This, in turn, is caused by a suction side flow separation from the main blade leading edge in the area close to the shroud (see Figs. **Fig. 11** and **Fig. 12** showing the velocity field at 95% impeller blade span, and, for comparison, Figs. **Fig. 13** and **Fig. 14** showing the same at 50% span). This low energy fluid then migrates across the channel from the suction side of the main blades and meets the pressure sides of the neighbouring main blade and splitter blade at different distances and, thus, with different energies. (shown in Fig. 11 and Fig. 12).

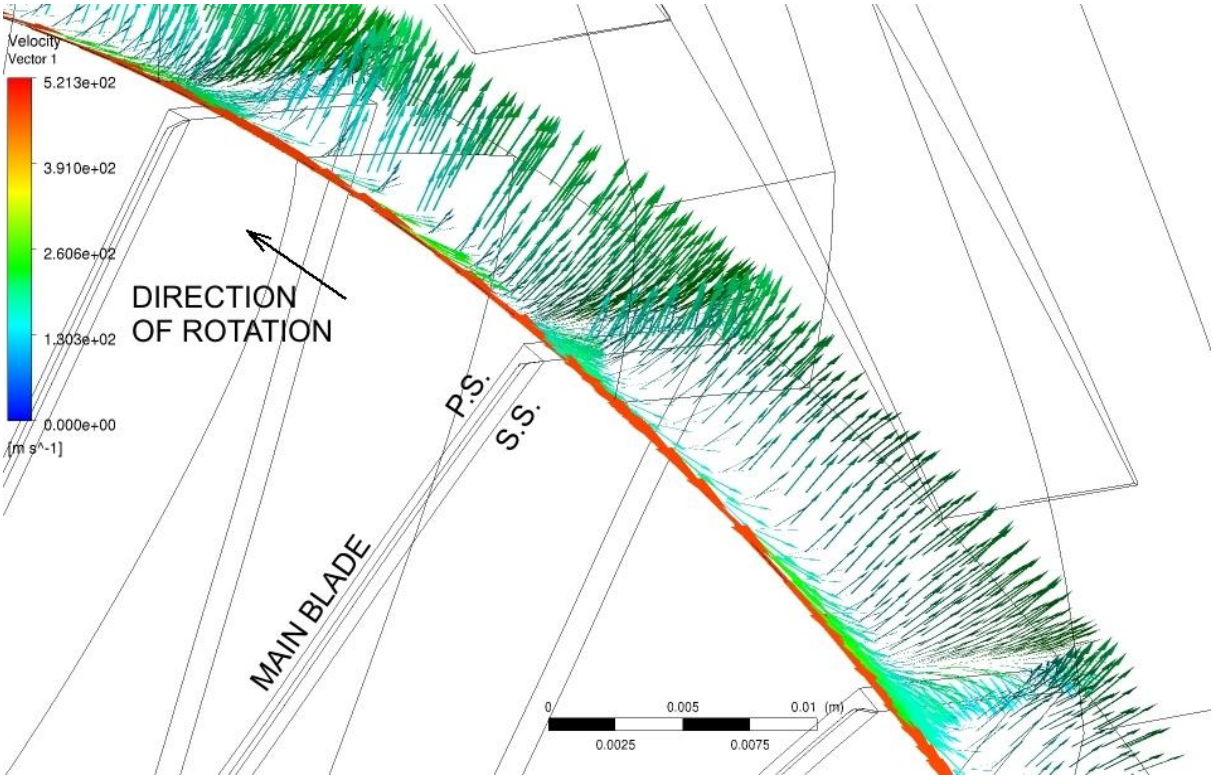

Fig. 9. *Vectors of relative velocity at impeller outlet*

5 Conclusions

In this paper, an initial computational model of a centrifugal compressor stage for aircraft engines was presented.

The results of the computations show that the model underestimates the isentropic efficiency as well as the total pressure ratio of the compressor stage. At the same time, the main phenomena determining the flow inside the impeller have been described and can be handled during the future development of this stage. The main problem the uneven distribution of pressure and velocity fields in the two sets of impeller channels caused by low-momentum fluid migrating across the channels and accumulating near the shroud and the suction sides of both sets of blades.

In the next stage of development which will follow after refining and calibrating the computational model, the tandem impeller blades will be introduced and their impact on flow field inside the stage, and on its total pressure ratio and isentropic efficiency of the stage will be investigated.

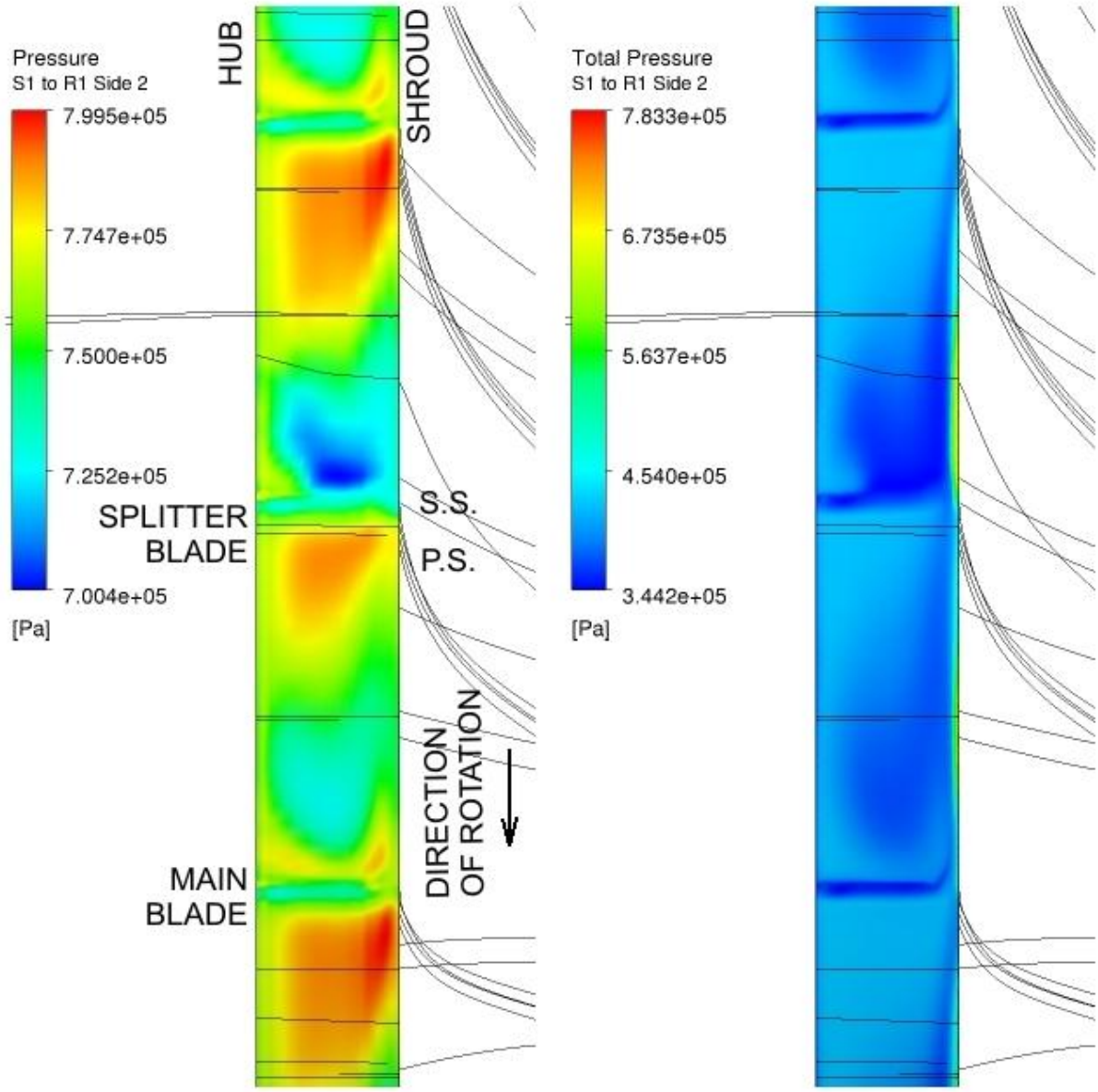

Fig. 10. *Pressure distributions at impeller exit. Left, static pressure. Right, total pressure.*

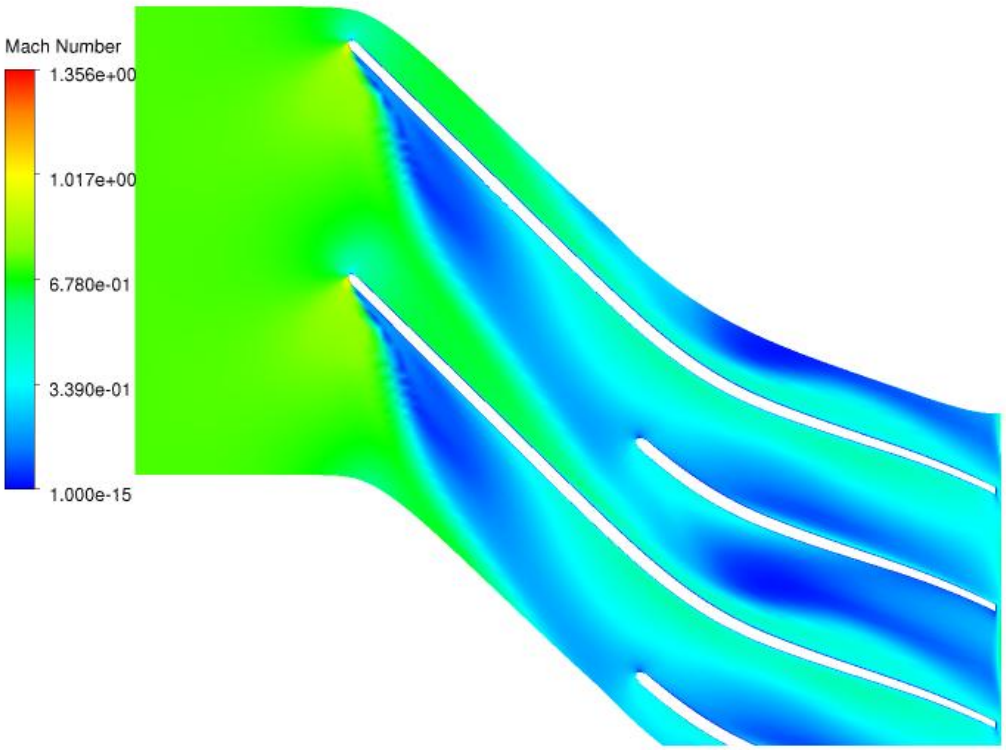

Fig. 11. *Relative velocity Mach number distribution inside the impeller, 95% span*

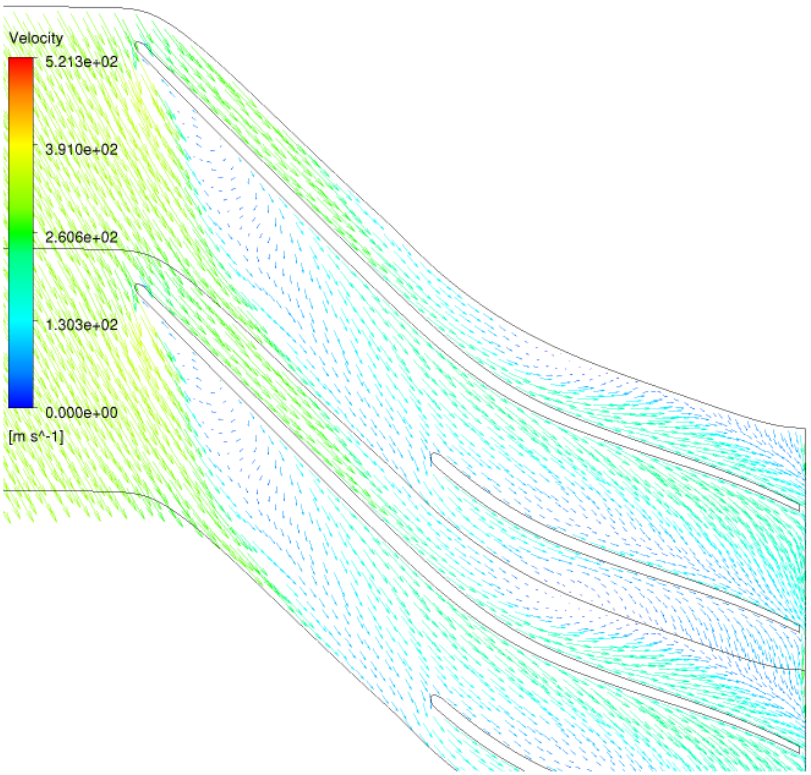

Fig. 12. *Relative velocity vectors inside the impeller, 95% span*

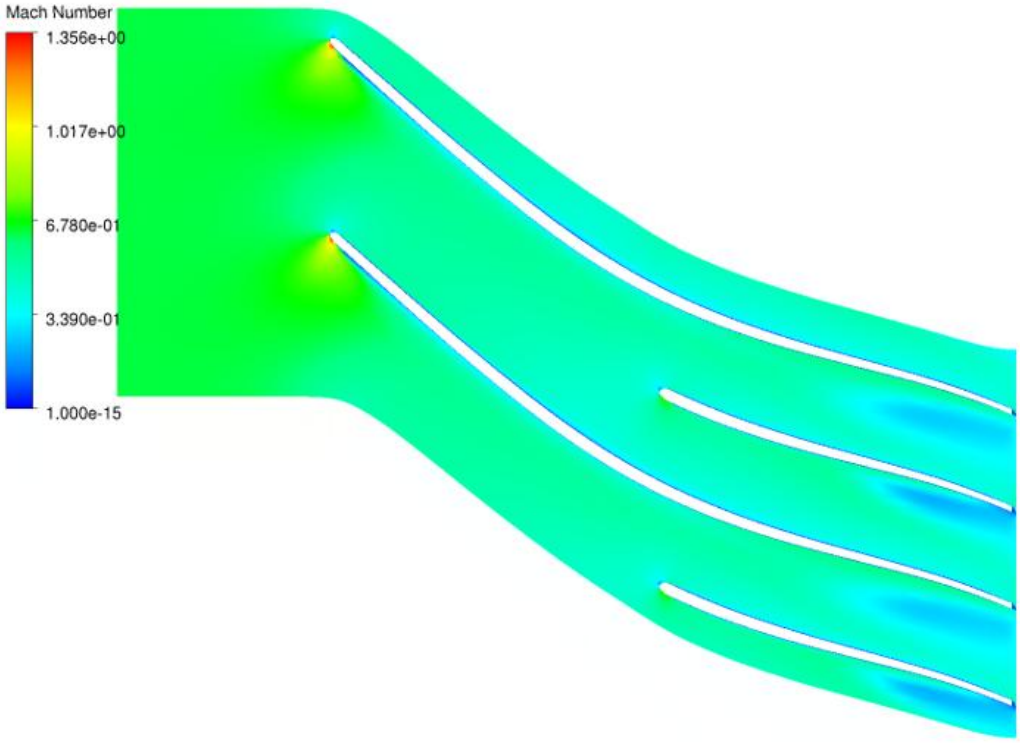

Fig. 13. *Relative velocity Mach number distribution inside the impeller, 50% span*

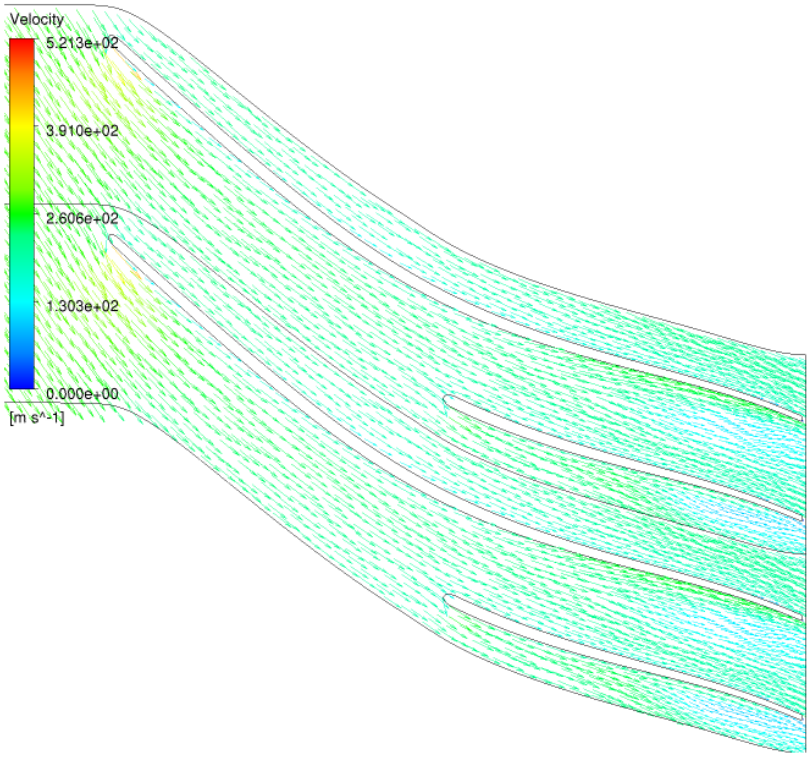

Fig. 14. *Relative velocity vectors inside the impeller, 50% span*

List of symbols

c_p	Specific heat capacity at constant pressure	($J.kg^{-1}.K^{-1}$)
C_μ	Constant (k-ε turbulence model)	(1)
k	Turbulent kinetic energy	($m^2.s^{-2}$)
n	Temperature exponent (Sutherland formula)	(1)
R	Constant (air specific heat capacity model)	($J.K^{-1}$)
S	Sutherland constant	(K)
T	Temperature	(K)
u^*	Shear velocity	($m.s^{-1}$)
y^+	Dimensionless distance from the wall	(1)
ε	Turbulent eddy dissipation	($m^2.s^{-3}$)
μ	Dynamic viscosity	(Pa.s)
μ_t	Turbulent viscosity	(Pa.s)
ν	Kinematic viscosity	($m^2.s^{-1}$)
ρ	Density	($kg.m^{-3}$)
τ_w	Wall shear stress	(Pa)

	Subscripts:
0	initial value
ref	reference value
eff	efficient value
w	value at the wall

References

[1] AGHAEI TOG, R. – TOUSI, A. M. – TOURANI, A. *Comparison of turbulence methods in CFD analysis of compressible flows in radial turbomachines*. In: Aircraft Engineering and Aerospace Technology. Vol. 80, Iss. 6, 2008. pp. 657-665. ISSN 1748-8842.

[2] *ANSYS CFX Modeling Guide*. Release 14.5.0. SAS IP, Inc. 2012.

[3] *ANSYS CFX Theory Guide*. Release 14.5.0. SAS IP, Inc. 2012.

[4] BATURIN, O.V. – KOLMAKOVA, D. A. – MATVEJEV, V. N. *Issledovanije rabočego processa centroběžnogo kompressora s pomoščju čislennych metodov gazovoj dinamiki* [*Исследование рабочего процесса центробежного компрессора с помощью численных методов газовой динамики*]. Samara: SGAU, 2013. 160 s.

[5] DENTON, John D. *Some limitations of turbomachinery CFD*. In: Proceedings of ASME Turbo Expo 2010: Power for Land, Sea and Air. Glasgow, 2010.

[6] DING, Ming Yao et al. *CFD Analysis of Off-design Centrifugal Compressor Operation and Performance*. In: 2006 International ANSYS Conference. Pittsburgh, 2006.

[7] HANUS, Daniel et al. *First stage of the centrifugal compressor design with tandem rotor blades*. In: Proceedings of ISABE 2005. München, 2005.

[8] LIU, Zheji – HILL, D.L. *Issues surrounding multiple frames of reference models for turbo compressor applications*. In: International Compressor Engineering Conference, 2000.